Advanced Materials

ADVANCED MATERIALS
www.advmat.de

RESEARCH ARTICLE

High-Contrast Handedness Inversion in Circularly Polarized Organic Ultralong Phosphorescence Enabled by an Antagonistic Chirality-Offset Helical Superstructure

Chi-Bo Feng[1] | Juan Wei[2] | Jiao Liu[1] | Wen-Lei Duan[1] | Xin-Yi Du[1] | Hao-Yi Jiang[1] | Fei Xu[1] | Zi-Ye Wang[1] | Yun Ma[1,2] | Bing-Xiang Li[1,2] | Yan-Qing Lu[3] | Qiang Zhao[1,2]

[1]College of Electronic and Optical Engineering & College of Flexible Electronics (Future Technology), Nanjing University of Posts and Telecommunications, Nanjing, China | [2]State Key Laboratory of Flexible Electronics (LoFE) & Institute of Advanced Materials (IAM), Nanjing University of Posts and Telecommunications, Nanjing, China | [3]National Laboratory of Solid State Microstructures & Collaborative Innovation Center of Advanced Microstructures & College of Engineering and Applied Sciences, Nanjing University, Nanjing, China

Correspondence: Yun Ma (iamyma@njupt.edu.cn) | Bing-Xiang Li (bxli@njupt.edu.cn) | Yan-Qing Lu (yqlu@nju.edu.cn) | Qiang Zhao (iamqzhao@njupt.edu.cn)

Received: 26 January 2026 | **Revised:** 25 April 2026 | **Accepted:** 12 May 2026

Keywords: materials science | phosphorescence | photoswitch

ABSTRACT

Dynamic and reversible control of circularly polarized ultralong room-temperature phosphorescence (CP-OURTP) is highly desirable for time-gated chiroptical photonics. Yet, the simultaneous realization of handedness inversion and large dissymmetry factors remains challenging because inversion typically occurs near a net-chirality cancellation point where the photonic bandgap (PBG) collapses. Here, we report a decoupled bilayer CP-OURTP film that couples a room-temperature phosphorescent polymer emitter with a photoresponsive chiral helical superstructure (CHS) engineered by an antagonistic chirality-offset design. By pairing a high-HTP chiral photoswitch with an oppositely handed static dopant, the net HTP reversibly crosses zero while remaining comparable in magnitude in the two photostationary states, thereby maintaining a robust PBG-emission overlap on both sides of inversion. Consequently, the film delivers reversibly switchable g_{lum} up to ±1.0 under alternating 365 and 530 nm irradiation, together with a phosphorescence quantum yield of 21.4%, an ultralong lifetime up to 388 ms, and stable operation over 50 switching cycles. The combined CP-OURTP and selective circular-polarization reflection enable high-fidelity rewritable anti-counterfeiting labels. This CHS-engineering strategy provides a general route to CP-OURTP materials with on-demand chiroptical control for multi-level information encryption and smart photonic devices.

1 | Introduction

The ability to dynamically and reversibly control chiroptical luminescence is key to next-generation photonic technologies, and is highly sought after for applications ranging from high-security anti-counterfeiting and rewritable optical data storage to advanced 3D displays [1–5]. Among various luminescent phenomena, circularly polarized organic ultralong room-temperature phosphorescence (CP-OURTP) is emerging as a particularly powerful platform [6–13]. Ultralong phosphorescence describes a luminescence process that persists even after the excitation source is removed, with a lifetime exceeding 0.1 s. By harnessing its intrinsic long-lived afterglow, CP-OURTP adds a temporal dimension to the chiroptical landscape, enabling time-gated signal readout and multi-level information encryption that are inaccessible to prompt fluorescent systems. However,

Chi-Bo Feng, Juan Wei and Jiao Liu contributed equally to this work.

the practical realization of these concepts has been hindered by a persistent materials challenge. It remains difficult to create systems that integrate high dissymmetry factors (g_{lum}) for clear signal distinction, ultralong lifetimes for effective temporal gating, and dynamic chirality switching for on-demand information processing.

Chiral nematic liquid crystals (CLCs) [2, 14–22] provide a powerful strategy to achieve high g_{lum} values in CP-OURTP systems [11, 19, 23–26]. Their periodic helical superstructure creates a photonic bandgap (PBG) that selectively reflects one handedness of circularly polarized light [16, 17], effectively amplifying the dissymmetry of embedded phosphorescence when the PBG spectrally overlaps with it. Building on this principle, our group previously demonstrated dynamic g_{lum} tuning from 0.60 to 1.38 by incorporating a light-driven molecular motor [4] into a CLC matrix [27, 28]. This modulation, however, was confined to a single handedness, as the unidirectional rotation of the motor continuously altered the helical pitch but could not cross the zero-chirality point to invert the helix. Subsequent use of chiral photoswitches did achieve full handedness inversion for binary "+/−" signal switching, yet these systems suffered from a severe performance trade-off arising from the low helical twisting power (HTP) [22] of the photoswitch and a spectral mismatch between the PBG and the phosphorescence emission [1]. This highlights a central dilemma in the field that achieving dynamic handedness inversion often comes at the cost of a markedly reduced g_{lum}. Therefore, developing a material system that breaks this trade-off and delivers both complete chirality inversion and exceptionally high g_{lum} values remain a pivotal and formidable challenge essential for high-fidelity chiroptical switching in advanced information technologies.

Herein, we overcome this performance issue by developing a novel photo-responsive chiral helical superstructure (CHS). The core of this work is a synergistic pairing within the CHS layer, combining a high-performance chiral photoswitch (CHAD-3C-R) [29] with a static chiral dopant (S5011) of opposite handedness. This meticulously engineered pairing generates a large and controllable light-induced swing in the net HTP, which drives complete, robust, and fully reversible handedness inversion of the superstructure. As a result, the CP-OURTP film exhibits an exceptionally high g_{lum} that can be switched reversibly up to ±1.0, while maintaining a long-lived phosphorescence lifetime of 388 ms and fatigue resistance over more than 50 cycles. Based on these chiroptical properties, we demonstrate high-fidelity photowriting and erasing of complex CP-OURTP patterns, indicating strong potential for advanced anti-counterfeiting and rewritable optical memory. This work thus presents a powerful and versatile CHS-engineering strategy for creating intelligent CP-OURTP materials with on-demand chiroptical control, paving the way for real-world photonic applications.

2 | Results and Discussion

2.1 | Design and Fabrication of the CP-OURTP Bilayer System

To achieve binary switching of CP-OURTP with a large g_{lum}, the chiral photonic structure must satisfy two seemingly conflicting requirements: (i) undergoing complete handedness inversion, and critically, (ii) maintaining a strong spectral overlap between the PBG and the phosphorescence emission in both handedness states. In conventional photoswitchable CLC systems, handedness inversion often occurs near a net-chirality cancellation point, where the helical pitch diverges and the PBG effectively vanishes, leading to a pronounced collapse of g_{lum}. To break this trade-off, we designed a decoupled bilayer architecture in which a photoresponsive CHS serves as the switchable chiroptical amplifier, while a room-temperature phosphorescent polymer (P1) acts as a stable and long-lived emitter [30].

The CHS layer functions as a chiroptical engine. It was formulated using a multicomponent nematic host (HTW114200-050, 85.1 wt.%) doped with a high-performance chiral photoswitch, CHAD-3C-R (12.5 wt.%), and an oppositely handed static chiral dopant, S5011 (2.4 wt.%) (Figure 1a). The choice of the nematic host is pivotal for realizing a reproducible, switchable CHS at such high dopant loading. Unlike single-component hosts, the eutectic mixture HTW114200-050 that comprises cyanobiphenyls, esters, and high-birefringence tolanes, offers broader compositional tolerance (Figure S1). This compatibility is crucial for stabilizing the high concentrations of both CHAD-3C-R and S5011, thereby suppressing phase separation and preserving a uniform LC texture. Furthermore, its large birefringence facilitates a broad and reflective PBG, ensuring effective photon management during pitch modulation.

Our key design rule employs an antagonistic chirality-offset strategy. Specifically, an oppositely handed static dopant is introduced to offset the photoswitch such that the net HTP reverses sign upon photoisomerization while remaining comparable in absolute magnitude (theoretically targeting symmetrical values of +1.14 vs. −1.17 μm^{-1}). This striking symmetry maintains a robust PBG in both handedness states, allowing persistent PBG-emission overlap and thus enabling symmetric switching of g_{lum} approaching unity (±1.0). The experimental validation of this photoinduced HTP evolution is quantified in the following section.

P1 was selected as the emissive layer because polymer-chain confinement effectively restricts molecular motions and suppresses non-radiative deactivation, providing a stable ultralong afterglow. The bilayer geometry further decouples the chiral photonic modulation from the emissive layer, allowing independent optimization of afterglow performance and chiroptical amplification. With this formulation, the photoisomerization of chiral photoswitches CHAD-3C-R continuously modulates the helical pitch, translating into a large, reversible shift of the PBG. Employing light as an external stimulus to modulate dynamic LC systems enables spatiotemporal accuracy. The most efficient method to encode the photoresponsive behavior of chiral LCs involves incorporating small, light-sensitive molecules—specifically photoswitches—as (chiral) dopants, enabling fine-tuning and regulation of the optical characteristics of LC materials. Azobenzenes [3, 31–35], dithienylethenes [22, 36–38], and overcrowded alkene molecular motors [39] functionalized with external chiral moieties have significantly enhanced photoresponsive LC systems. These compounds demonstrate considerable potential in controlling the winding and unwinding of helical architectures and facilitating handedness reversal in CLC systems. Hydrazone-based switches

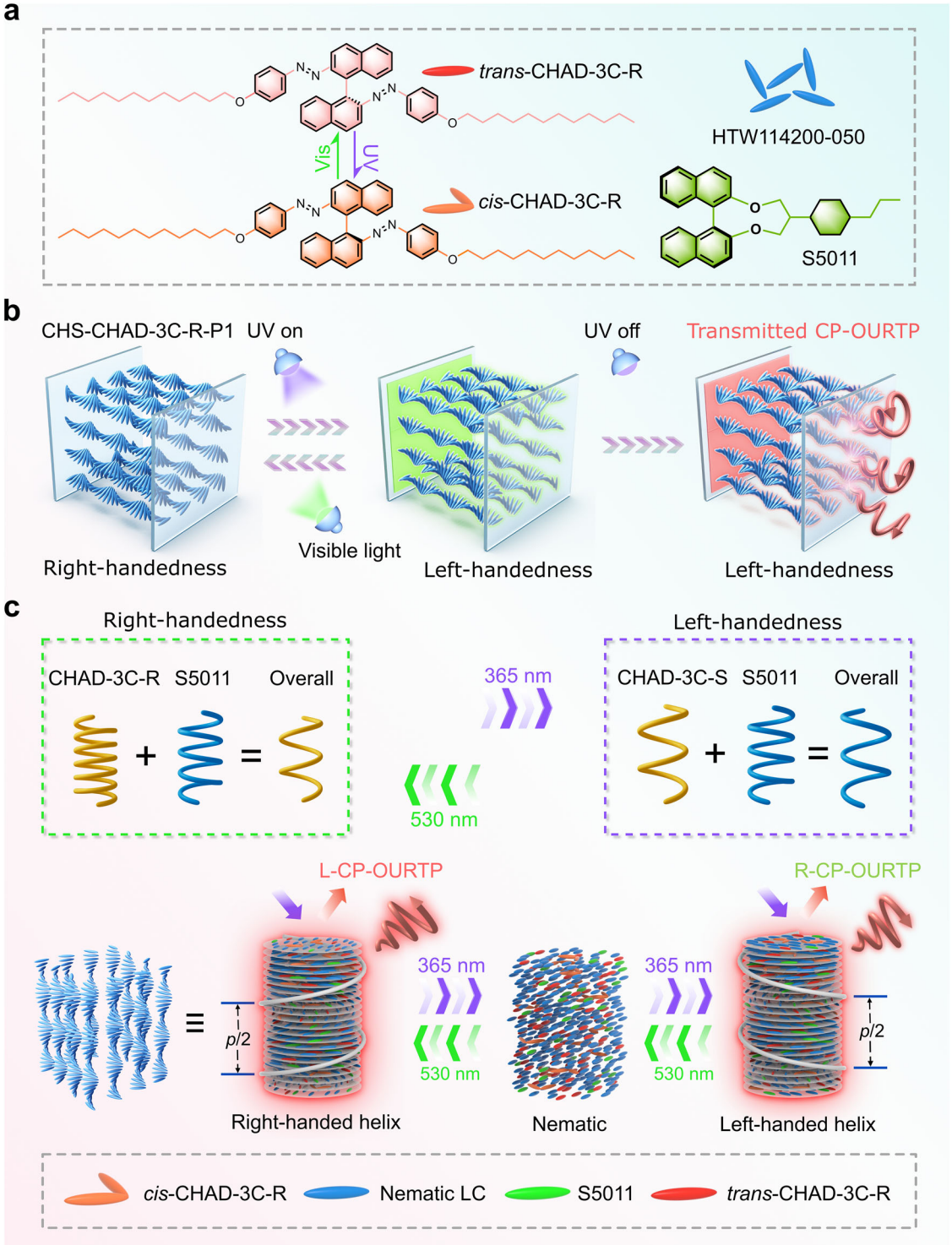

FIGURE 1 | Schematic illustration of dynamic chirality inversion in circularly polarized organic ultralong room-temperature phosphorescence (CP-OURTP) based on chiral helical superstructures. (a) Chemical structures of the materials made for the CP-OURTP bilayer film. (b) Schematic diagram of dynamic chirality inversion in CP-OURTP bilayer film. (c) Schematic illustrations of CLC superstructure evolution driven by 365 nm UV and 530 nm visible light.

containing chiral components have shown promising potential in modulating the HTP values [40–42]. Incorporating these photoactive chiral molecules into CLCs allows for accurate, non-contact regulation of helical superstructures, enabling effective tuning of their reflective band properties. Although the variations in HTP induced by current photoresponsive dopants are generally small, very few systems are capable of achieving helicity inversion in existing LC materials. Modifying significant HTP values alongside enabling helicity inversion is crucial for advancing LC systems in next-generation smart material applications, particularly in sophisticated areas like camouflage coloration and data encryption. In this work, CHAD-3C-R is a

high-HTP chiral photoswitch whose HTP changes significantly upon photoisomerization. When combined with the oppositely handed static chiral dopant S5011, this large HTP swing enables the net HTP of the system to cross zero and reverse sign, while remaining comparable in absolute magnitude in the two photostationary states (+1.14 vs. −1.17 μm^{-1}). This behavior is fundamentally important because it allows complete handedness inversion of the CHS without collapsing the PBG, thereby preserving the PBG–emission overlap required for high g_{lum} values. By contrast, although many widely used photoswitches in cholesteric systems are employed to modulate pitch or reflection wavelength through photoinduced configurational change as mentioned above, they often do not simultaneously provide both a sufficiently large HTP swing and a balanced net chirality on both sides of inversion. The role of CHAD-3C-R is distinguished not only by its photoresponsiveness, but also by its compatibility with the antagonistic chirality-offset strategy that preserves robust chiroptical amplification during inversion. We next quantify this photoinduced evolution and the associated chirality inversion via reflection spectroscopy and circular-polarization-resolved measurements (Figure 2).

2.2 | Dynamic Switching of Photonic Bandgap and Chirality

To investigate the optical characteristics of the CP-OURTP bilayered film, various optical conditions were performed. First, the dynamic modulation of the photonic band gaps (PBGs) was conducted by exposing the CHS-CHAD-3C-R-P1 to 365 nm UV light irradiation (50 mW cm^{-2}) and then irradiating the sample with a 530 nm visible light source (37 mW cm^{-2}) in a planar LC cell, respectively (Figure 2a,b). The PBG of the heliconical CHS can be dynamically and reversibly manipulated by controlling the irradiation time of UV and visible light, which covers a wide spectral range from visible to the near-infrared (NIR) range (Figure 2a,b). The overall reflection colors changed significantly as the increase of the UV irradiation time due to the alteration of the helical pitch of the CHS (Figure S2). With increasing UV irradiation time from 0 s to 90 s, the initial reflection band gradually red-shifted from 550 to 920 nm, followed by a blueshift from 920 to 680 nm upon further irradiation from 90 to 120 s (Figure 2a). Notably, the PBGs return to their initial state after visible light irradiation for 120 s (Figure 2b). Furthermore, the reflection spectra of the CHS-CHAD-3C-R-P1 in the initial state under left-handed circularly polarized filter (L-CPF) and right-handed circularly polarized filter (R-CPF) indicate that the sample is right-handed in the initial state (Figure 2c and Figure S3). Subsequently, the sample gradually transitions to the left-handedness after the irradiation of 365 nm UV light to the photostationary (PSS_{365}) state, and finally recovers to the initial right-handedness after the irradiation of 530 nm visible light to photostationary (PSS_{530}) state (Figure 2d and Figure S4). Moreover, the reflection polarized optical microscopy (POM) images under L-CPF and R-CPF further confirm that the chirality of the CHS-CHAD-3C-R-P1 inverts from the right-handedness to the left-handedness upon irradiating by 365 nm UV light to the PSS_{365} state and then changes to the right-handedness in PSS_{530} state (Figure 2e and Figure S5). The observed oily streak textures in transmission POM images illustrate that the initial self-organized helical superstructures of the CHS are maintained after the complete irradiation of light with different wavelengths (Figures S6 and S7). It is observed that under continuous irradiation of 530 nm light, the reflection POM images under R-CPF are brighter than those under L-CPF, signifying that the CHS-CHAD-3C-R-P1 sample inverts from the left-handed to the right-handed state (Figure S5). Moreover, the effect of the thickness of the CHS on the position of the PBGs was also investigated (Figure S8), and the reflection spectra show that the thickness of the CHS does not impact the position of the PBGs significantly. Therefore, by alternating light source with different wavelengths, the reversible dynamic modulation of the reflection bands and dynamic chirality inversion manipulation for the CHS-CHAD-3C-R-P1 sample can be achieved in a planar LC cell. Similarly, the optical characteristics of the CHS-CHAD-3C-R-P1 sample in homeotropic LC cells were also investigated, and the similar results show that the dynamic modulation of PBGs and chirality inversion can also be achieved under the alternating of light sources with different wavelengths (Figures S9–S17).

2.3 | Chiroptical Properties of the CP-OURTP Film

The prepared CHS-CHAD-3C-R-P1 film can be applied to optical labels. The photographs of the CP-OURTP emission under no CPF, L-CPF, and R-CPF upon the irradiation of 365 nm UV light for different periods of time and then switching off UV light were captured to provide a comprehensive understanding of the chiroptical properties of the CHS-CHAD-3C-R-P1. The CHS-CHAD-3C-R-P1 film was exposed to the UV light for 0, 10, 20, 30, 90, 100, and 120 s, respectively. It was found that in the initial state, the red afterglow emitted from the CHS-CHAD-3C-R-P1 sample under L-CPF is more pronounced than that under R-CPF, which is ascribed to the inherent right-handed structures of the CHS-CHAD-3C-R-P1. After the irradiation for 30 s, the light-triggered helix deformations shift the optical state from right-handed circular polarization to left-handed circular polarization, as evidenced by that the red afterglow emission under R-CPF is stronger than that under L-CPF (Figure 3a,c). Concretely, under the irradiation of 365 nm UV light, the CHAD-3C-R experiences the isomerization from *trans*-state to *cis*-state, resulting in the chirality inversion of the CHS-CHAD-3C-R-P1 sample from the initial right-handedness to left-handedness. Figure 3b depicts the normalized steady-state photoluminescence (PL), and delayed PL spectra of the room-temperature phosphorescence (RTP) polymer of P1. The PL spectra reflect the luminescent color of P1 and its phosphorescence emission with a maximum peak at 630 nm. Furthermore, the decay curve of the CP-OURTP film shows an ultralong lifetime of 388 ms (Figure 3d) and the phosphorescence quantum yield is 21.39% (Figure S18).

To further investigate the dynamic chirality inversion process of the bilayer CP-OURTP film, the PBG of the CHS is purposely controlled to overlap with the emission band of P1 to achieve a high g_{lum} value. The chiroptical activities of the CHS-CHAD-3C-R-P1 film were evaluated by the ground-state circular dichroism (CD) and excited-state circularly polarized luminescence (CPL) spectroscopy, respectively. The luminescence dissymmetry factor (g_{lum}), expressed as $g_{lum} = 2 \times (I_L - I_R)/(I_L + I_R)$, is a critical parameter for assessing the extent of circularly polarized luminescence, where I_L and I_R denote the intensities of left- and right-handed circularly polarized emission, respectively.

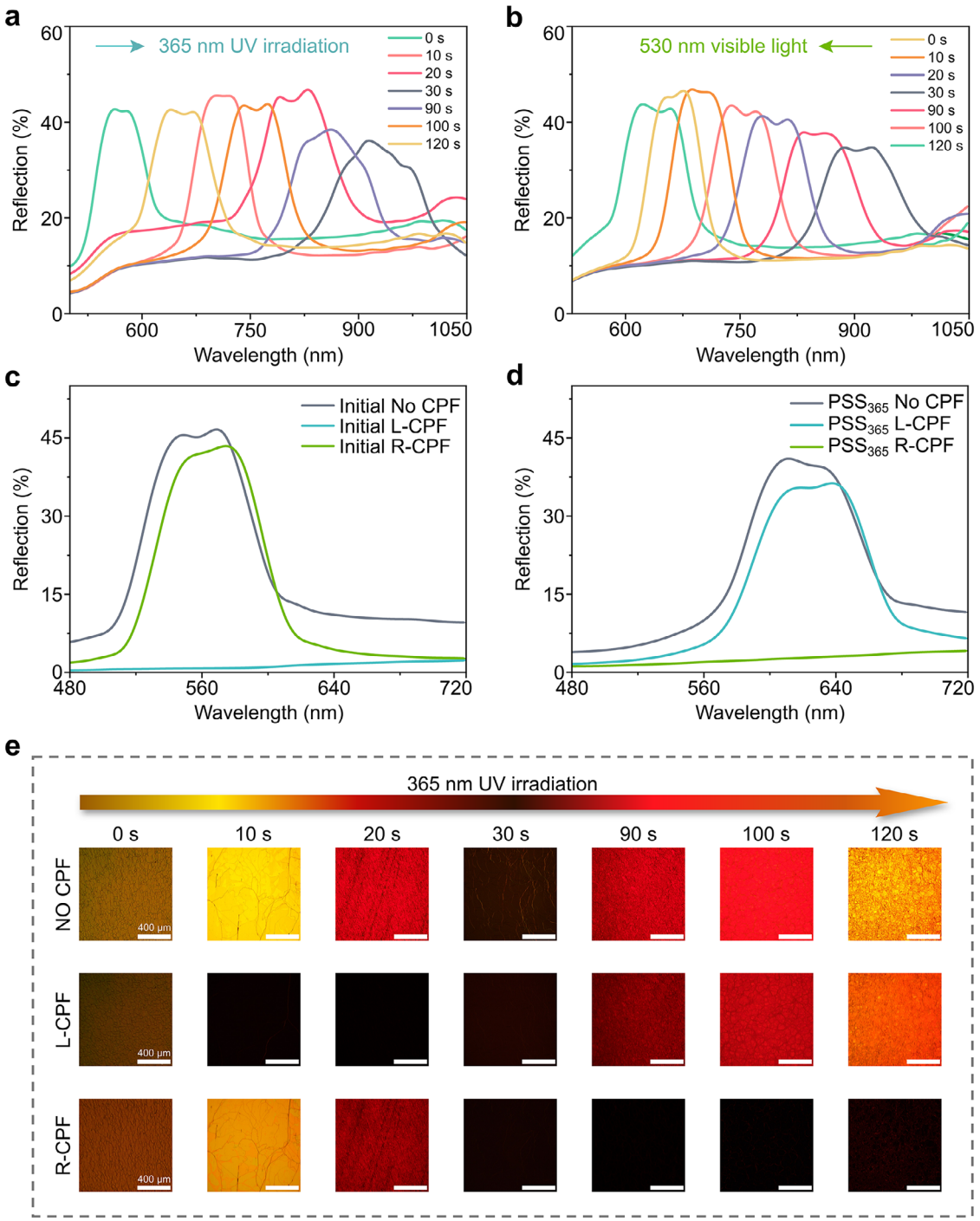

FIGURE 2 | Dynamic modulation of the photonic band gaps (PBGs) and chirality inversion of the bilayer CP-OURTP film based on chiral helical superstructure (CHS). (a,b) Reflection band modulation of the CHS-CHAD-3C-R-P1 sample under 365 nm UV light irradiation (a) and return to its initial state under 530 nm visible light irradiation (b) in a planar LC cell. (c,d) Reflection band of the CHS-CHAD-3C-R-P1 cell under the irradiation of 365 nm UV light in the initial state (c) and PSS_{365} state (d) under no circularly polarized filter (CPF), left-handed circularly polarized filter (L-CPF), and right-handed circularly polarized filter (R-CPF) in a planar LC, respectively. (e) Reflection polarized optical microscopy (POM) images of CHS-CHAD-3C-R-P1 upon irradiating by UV light for different periods of time under no CPF, L-CPF, and R-CPF, respectively. The thickness of the LC cell is 23.0 μm. All scale bars are 400 μm.

Experimentally, g_{lum} is given by the equation $g_{lum} = \frac{\text{ellipticity (mdeg)}}{(32980/\ln 10)\times \text{PL (DC in volts)}}$ at the CPL extremum. This formula shows that the g_{lum} values depend on both the CPL intensity and the DC voltage, implying that a higher CPL intensity does not guarantee a higher g_{lum} value. The CD spectroscopy was used to measure the light-triggered chirality inversion of the bilayer CHS-CHAD-3C-R-P1 film, which displays a negative absorption band between 500 and 600 nm in a planar LC cell (Figure 4a). Notably, the intensity of the CD signal for the CHS-CHAD-3C-R-P1 under the

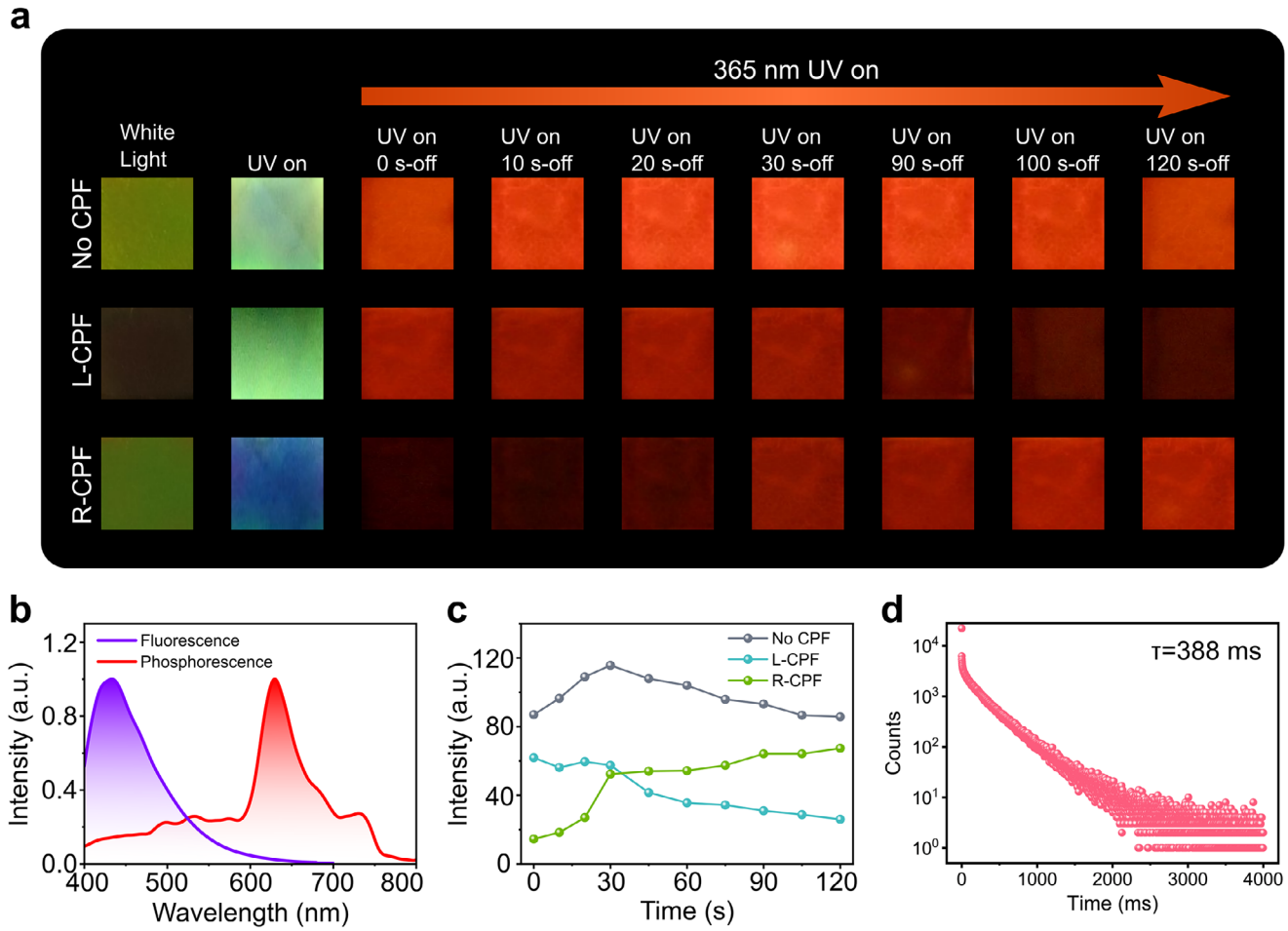

FIGURE 3 | (a) Photographs of the CHS-CHAD-3C-R-P1 sample with red afterglow taken under white light, 365 nm UV light irradiation for different periods of time, and switching off UV light under no CPF, L-CPF, and R-CPF, respectively. (b) The steady-state photoluminescence (PL) and delayed PL emission spectra of P1. (c) The afterglow intensity decay curves of the CHS-CHAD-3C-R-P1 sample under no CPF, L-CPF, and R-CPF, respectively. (d) The decay curve of the CHS-CHAD-3C-R-P1.

irradiation of light with different wavelengths exceeds the spectral range due to the chirality amplification effect of the CHS (Figure 4a,d). When the CHAD-3C-R was activated by 365 nm UV light to the PSS_{365} state, the negative absorption peak at 500–600 nm disappears and a new positive absorption band between 620 and 700 nm emerges, providing direct evidence of the chirality inversion for the CHS-CHAD-3C-R-P1 sample that inverts from the right-handedness to the left-handedness. Subsequently, when the sample was under the continuous irradiation of 530 nm visible light to PSS_{530} state, the negative absorption band at around 600 nm reappears, revealing that the CHS-CHAD-3C-R-P1 reverts to its original right-handed state under the irradiation of 530 nm visible light (Figure 4a). Furthermore, the CPL spectroscopy was employed to investigate the light-driven chirality inversion of the CHS-CHAD-3C-R-P1 sample. The CPL typically denotes the difference in emission intensities in left- and right-handed circularly polarized light produced by chiral luminescent systems when excited. The degree of CPL is quantified by the g_{lum} value, defined as $g_{lum} = 2 \times (I_L - I_R)/(I_L + I_R)$, where I_L and I_R represent the intensities of the left and right circularly polarized emissions, respectively [24, 43–46]. Experimentally, the value of g_{lum} is defined as $g_{lum} = \frac{\text{ellipticity (mdeg)}}{(32980/\ln 10)\times\text{PL (DC in volts)}}$ at the CPL extremum. According to this equation, the g_{lum} values are determined by both the CPL intensity and DC in volts, indicating that a high CPL intensity does not necessarily lead to a high g_{lum} value. According to the equation, the maximum absolute value of g_{lum} is 2.0 [47, 48]. The circularly polarized phosphorescence (CPP) intensity and the g_{lum} values of the sample gradually decrease under the continuous irradiation of 365 nm UV light (Figure 4b,c). As the irradiation time increases to 30 s, the CPP signals with the opposite g_{lum} values were obtained, indicating the occurrence of chirality inversion of the CHS-CHAD-3C-R-P1 sample in a planar LC cell. As anticipated, the similar results of CD and CPP signals were achieved for the CHS-CHAD-3C-R-P1 in a homeotropic LC cell (Figure 4d–f). Moreover, the thermal stability of the CP-OURTP bilayer films under the irradiation of light with different wavelengths was investigated in both planar and homeotropic LC cells, respectively (Figure 4g,h), and the process can be repeated for 50 cycles without any fatigue. Figure 4i is the comparison of lifetime and g_{lum} value regulation in the previously reported CPL assemblies. The bilayer film enables the dynamic chirality inversion in CP-OURTP, exhibiting a reversibly switchable g_{lum} of up to ±1.0 under alternating 365 nm UV and 530 nm light irradiation.

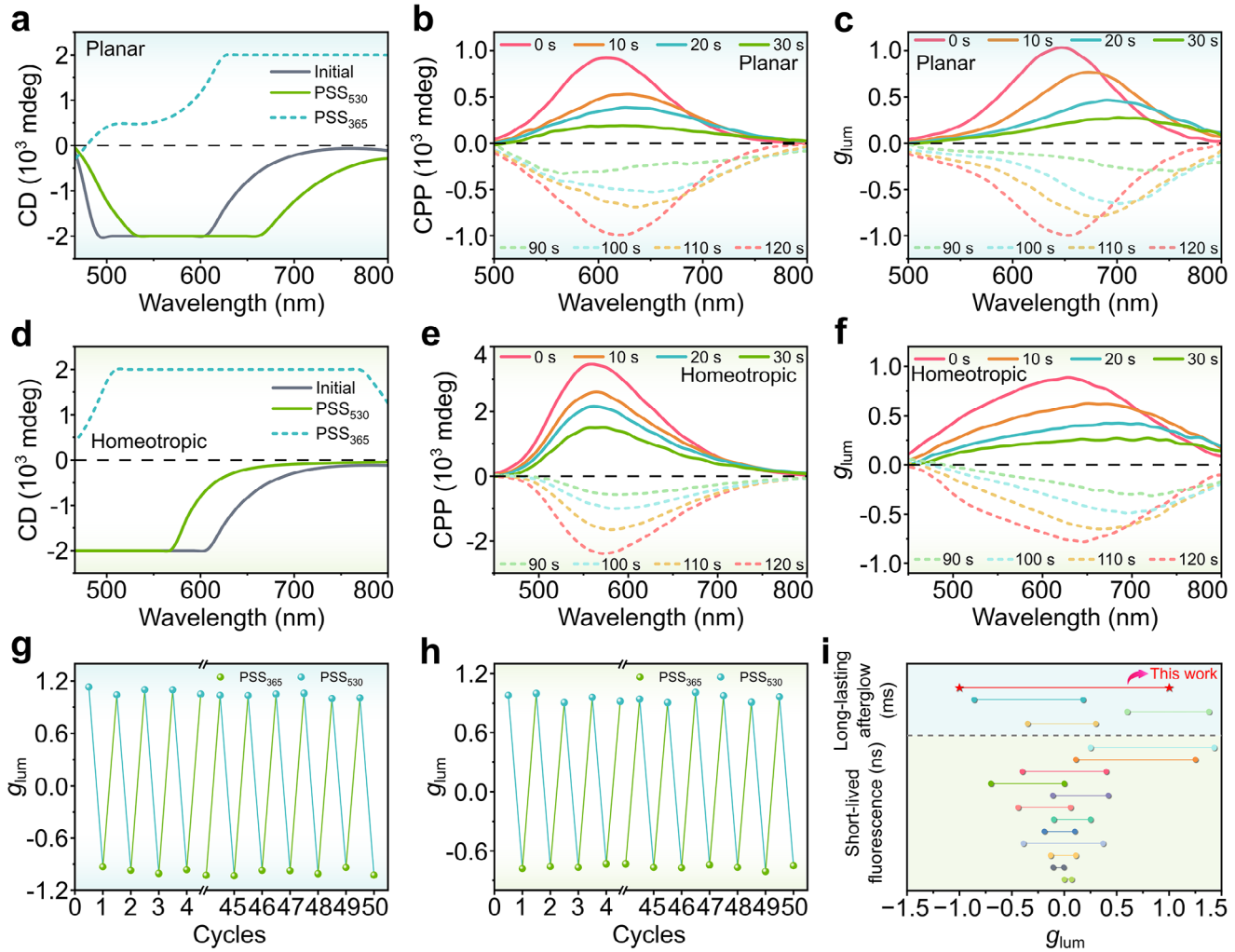

FIGURE 4 | Chirality inversion of the CP-OURTP bilayer films. (a) Circular dichroism (CD) spectra of the CHS-CHAD-3C-R-P1 sample in the initial state, PSS_{365}, and PSS_{530} in a planar LC cell, respectively. (b,c) Circularly polarized phosphorescence (CPP) signals (b) and the g_{lum} curves (c) of the CHS-CHAD-3C-R-P1 under 365 nm UV light irradiation for different periods of time in a planar LC cell. (d) CD spectra of the CHS-CHAD-3C-R-P1 film in the initial state, PSS_{365}, and PSS_{530} in a homeotropic LC cell, respectively. (e,f) CPP signals (e) and the g_{lum} curves (f) of the CHS-CHAD-3C-R-P1 under 365 nm UV light irradiation for different periods of time in a homeotropic LC cell. (g,h) Cycling test of the g_{lum} values for the CHS-CHAD-3C-R-P1 film in PSS_{365} and PSS_{530} in a planar and homeotropic LC cell, respectively. (i) Comparison of lifetime and g_{lum} value regulation in the circularly polarized luminescence assemblies. The LC cell thickness is 23.0 μm.

The effect of the thickness of the CHS on the g_{lum} values was also investigated (Figure S19), and the results show that the thickness of the CHS between 16.0 and 37.4 μm does not impact the g_{lum} values significantly. Notably, this CP-OURTP system offers a significant advantage over previously reported tunable g_{lum} values, featuring both a wider range of g_{lum} value regulation and prolonged afterglow (The details are listed in Figure S20). The remarkably high g_{lum} value in this bilayer CP-OURTP film does not mainly originate from the RTP polymer itself, but from the chiral photonic amplification provided by the CHS. The periodic helical structure of the CHS can generate a PBG that selectively reflects one handedness of circularly polarized light, thereby amplifying the g_{lum} value when the PBG completely overlaps with the emission band of P1. More importantly, the antagonistic chirality-offset design enables the net HTP to reverse sign while remaining comparable in magnitude in the two photostationary states, which allows the CHS to maintain a robust PBG–emission overlap on both sides of handedness inversion. Therefore, the observed high g_{lum} is indeed closely related to the chirality effect of the CHS, but more precisely, it arises from the combined effects of selective circular-polarization reflection, chirality amplification, and the preserved PBG–emission overlap enabled by our antagonistic chirality-offset design. These results indicate that the light-triggered CHAD-3C-R can modulate the CPP signals and the g_{lum} values of the CHS-CHAD-3C-R-P1 film under the alternating irradiation of 365 nm UV light and 530 nm light, which demonstrate unique value in the field of encryption applications.

To evaluate the variation of HTP (β) of the CHAD-3C-R in different states, the Grandjean-Cano wedge method was employed by using the CHS-CHAD-3C-R (Figure 5). The helical pitch (p) represents the distance over which the LC director undergoes a 360° rotation around the helical axis. The HTP measures the ability of the chiral dopant to induce the twisting in a nematic LC, which can be determined by the equation below.

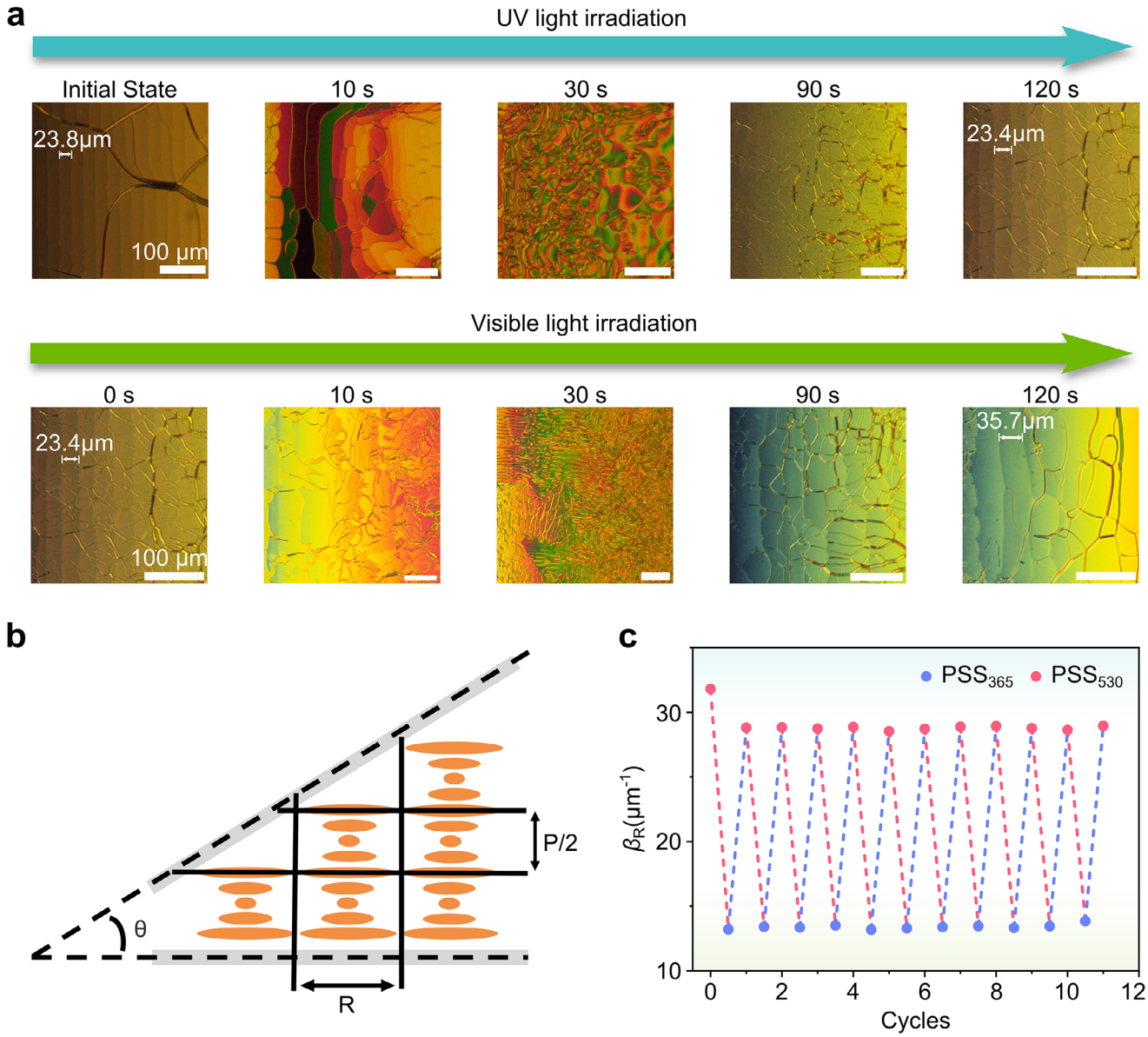

FIGURE 5 | Chirality inversion of the CHS-CHAD-3C-R sample sandwiched in a Grandjean-Cano wedge cell under the irradiation of UV and visible light. (a) Changes in the handedness of the CHS-CHAD-3C-R sample upon irradiation with UV light, followed by irradiation with 530 nm visible light. All scale bars are 100 μm. (b) Schematic illustration of a Grandjean-Cano wedge cell for measuring the pitch of CHS-CHAD-3C-R. (c) Cycling test of helical twisting power (β_R) of the CHAD-3C-R variations in PSS_{365} state (represented by blue ball) and PSS_{530} (denoted by red balls), respectively.

$$\beta = \frac{1}{pc} \tag{1}$$

where c is the concentration of CHAD-3C-R in LC host. The schematic illustration of Cano's wedge method is provided in Figure 5b. When the CLC was inserted into a wedge-shaped LC cell, the discontinuity lines (Cano lines) were observed under crossed polarizers. The p was calculated by measuring the distance (R) between the Cano lines, as described below.

$$p = 2R \tan\theta \tag{2}$$

where θ is the wedge angle of the cell. In this work, the wedge angle is $\tan\theta = 0.0183$. As a result, the β of the chiral dopant was calculated according to the following equation.

$$\beta = \frac{1}{2R \tan\theta c} \tag{3}$$

Upon UV irradiation, the CHAD-3C-R molecules undergo isomerization, transforming from a rod-like *trans* configuration to a bent *cis* configuration. Throughout the process of photoisomerization, there is a gradual reduction in β. Under the irradiation of 530 nm visible light, the reverse isomerization from *cis* to *trans* occurs slowly, while it can be significantly accelerated by the visible light illumination or heating. The p of the CHS can be calculated by,

$$p = \frac{1}{c_R \cdot \beta_R + c_S \cdot \beta_S} \tag{4}$$

where p is the helical pitch, c_R and c_S are the concentrations of CHAD-3C-R and S5011, and β_R and β_S are their respective HTPs. Notably, CHAD-3C-R was chosen because it combines a high initial HTP with a large photoinduced HTP swing: $\beta_R = 31.8\ \mu m^{-1}\ (wt.\%)^{-1}$ in the initial state and decreases to $13.3\ \mu m^{-1}\ (wt.\%)^{-1}$ upon UV irradiation, while S5011 provides a strong opposite contribution ($\beta_S = 118\ \mu m^{-1}\ (wt.\%)^{-1}$). Using the experimentally determined HTP values and the formulation employed in this work ($c_R = 0.125$, $c_S = 0.024$), Equation (4) predicts a positive net chirality in the initial state, $0.125 \times 31.8 - 0.024 \times 118 = +1.14\ \mu m^{-1}$, and a negative net chirality after UV-driven isomerization, $0.125 \times 13.3 - 0.024 \times 118 = -1.17\ \mu m^{-1}$. Importantly, the near-symmetric magnitude of the net chirality on both sides of inversion (+1.14 vs. −1.17 μm^{-1}) indicates that the CHS can sustain a robust PBG in both handedness states, rather than collapsing in one state as commonly observed in switchable systems. This symmetry provides the physical basis for maintaining PBG-emission overlap and thus enabling $\pm g_{lum}$ switching approaching unity.

2.4 | Application for Anti-Counterfeiting and Information Storage

Leveraging the combination of the chirality inversion of the CHS and phosphorescent properties of the RTP polymer, a photoresponsive helical LC system was developed by incorporating the chiral molecular switch and the chiral dopant into the nematic LC. Due to the excellent thermal stability of the chiral photoswitch of the CHAD-3C-R, any desired stable intermediate state along with its associated reflection color can be obtained. To further corroborate these findings, various patterned images were recorded in the photoresponsive CHS-CHAD-3C-R-P1 sample by using UV light and visible light to pass through different customized photomasks, the patterned images of "Chinese knot" with different reflection colors were obtained under UV light irradiation (Figure 6). The schematic diagram of chirality inversion in CP-OURTP through the predefined patterns is illustrated in Figure 6a. Interestingly, after switching off UV light, the red afterglow emission of the "Chinese knot" under L-CPF is brighter than that under R-CPF to the naked eye, indicating the intrinsic right-handed helical structures of the CHS-CHAD-3C-R-P1 sample. Subsequently, after exposure to 365 nm UV light for 20 s, no obvious difference of the emission was observed from the red "Chinese knot" under L-CPF and R-CPF, respectively. Notably, after illuminating the sample for 120 s by UV light, the afterglow emission from the "Chinese knot" under R-CPF was much stronger than that under L-CPF, elucidating the complete handedness inversion from the right-handedness to the left-handed state. Furthermore, the "Chinese knot" pattern can be maintained for 24 h under ambient condition and the images can be completely erased upon the irradiation of 530 nm visible light. In addition, different patterned images of "Temple of Heaven" can also be written and erased on the film by alternating the irradiation of UV light and visible light. To examine the stability, reproducibility, and efficiency of the encryption device in relation to the long-persistent luminescence characteristics, it was observed that the phosphorescence intensity and the lifetime experience only a minor decline after leaving alone for more than 30 days (Figure S21), which suggests that the encryption device demonstrates remarkable stability regarding the long-persistent luminescence characteristics. These results indicate that the chirality inversion in the CHS-CHAD-3C-R-P1 can be confirmed through the patterned films under the irradiation of light with different wavelengths.

3 | Conclusions

In conclusion, we demonstrated a switchable CP-OURTP bilayer that addresses the common trade-off between handedness inversion and high g_{lum} in photonic-assisted chiral systems. The central design principle is an antagonistic chirality-offset CHS: a high-HTP chiral photoswitch is counterbalanced by an oppositely handed static dopant so that photoisomerization drives the net HTP across zero without sacrificing its magnitude, thereby preserving a robust PBG-emission overlap in both handedness states. This enables reversible switching of g_{lum} up to ±1.0 while maintaining an ultralong afterglow lifetime up to 388 ms and good cycling stability. Beyond demonstrating rewritable anti-counterfeiting labels, the bilayer architecture decouples chiral photonic amplification from the emissive layer, offering a modular platform that can be extended to other emitters and stimuli-responsive CHS designs. We anticipate that this design rule will accelerate the development of time-gated chiroptical materials for multi-channel encryption, sensing, and smart photonic devices.

4 | Experimental Section

4.1 | Materials

All commercially available chemicals were used as received without further processing. The nematic LC HTW114200-050 and chiral dopant S5011 were all purchased from Jiangsu Hecheng Display Technology Co., Ltd The chiral molecular switch CHAD-3C-R was purchased from Jiangsu Hecheng Display Technology Co., Ltd. Polyvinyl alcohol (PVA-1799) was acquired from Shanghai Aladdin Biochemical Technology Co., Ltd. Dichloromethane (CH_2Cl_2, DCM) was purchased from Macklin. The wedge cells with parallel rubbing direction were purchased from EHC Co., Ltd, Japan. All the quartz substrates that are used for CPL measurement were acquired from Prism Optics. Glass substrates for preparation of LC cells were all obtained from Kaiwei photoelectric technology in Zhuhai.

4.2 | Fabrication of RTP-PVA Films

A mixture of the RTP polymer (P1, 50 mg) and PVA-1799 (200 mg) was dissolved in 2.5 mL deionized water vigorously stirred at 110°C for 2 h to obtain a uniform solution. The glass substrates with a length of 2 cm and a width of 2 cm were washed twice with deionized water and ethanol, respectively, followed by sonication for 10 min and dried at 95°C. Meanwhile, the prepared RTP-PVA solution was allowed to cool down to room temperature for further use. After that, the cleaned glass substrates were spin-coated with the RTP-PVA solution, and subsequently the solution was allowed to evaporate at 50°C in a vacuum oven overnight, followed by rubbing with a rayon cloth to ensure homogeneous alignment.

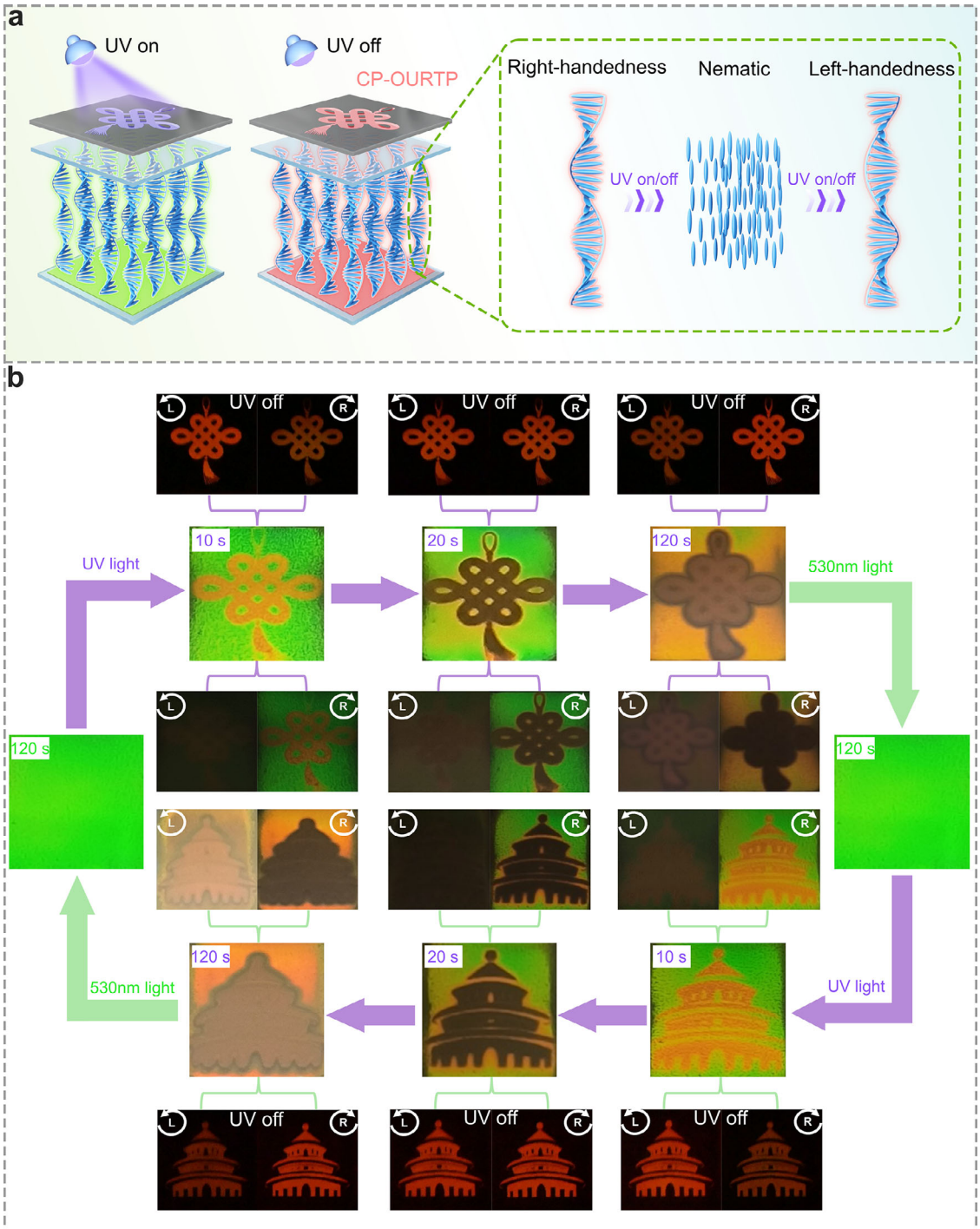

FIGURE 6 | Chirality inversion of the helical LC superstructures based on the CHS-CHAD-3C-R-P1 sample. (a) Schematic diagram of the chirality inversion in CP-OURTP through the predefined "Chinese knot" pattern. (b) Photowriting of the predefined patterns under irradiation of the UV light and erased by 530 nm light by passing through different photomasks.

4.3 | Fabrication of CHS-CHAD-3C-R-P1 Bilayered Films

A nematic LC HTW114200-050 (85.1 wt.%), a chiral photoswitch CHAD-3C-R (12.5 wt.%), and a chiral dopant S5011 (2.4 wt.%) were dissolved in 5 mL DCM. The CHS was obtained after evaporating the solvent completely at 70°C. Subsequently, one glass substrate was precoated with an RTP-PVA film and assembled with another cleaned planar alignment glass substrate to make an LC cell. The cell's thickness was controlled by using 25.0 μm spacer doped with UV glue. Similarly, another cleaned glass substrate was coated with P1-PVA film and assembled with a different cleaned glass substrate with homeotropic alignment, also controlled by 25.0 μm spacer doped with UV glue. The CHAD-3C-R-doped nematic LC was injected into the LC cell to fabricate the CHS-CHAD-3C-R-P1 film with the planar and homeotropic alignment, respectively,

followed by exposing the samples to light with different excitation wavelengths.

4.4 | Characterizations

Polarized optical microscopy (Nikon Ci-POL, Nikon company), optical spectrometer (PG2000-Pro, Shanghai Fu enjoy optics), hot stage (TS102XY), temperature controller (mK2000B), camera (Nikon Z50), circular dichroism spectrometer (JASCO J-810), circularly polarized luminometer (JASCO CPL-300), and steady-state phosphorescence spectra (Hitachi F-4700), lifetime measurements performed by using an Edinburgh FLS980 fluorescence spectrophotometer, which is equipped with a microsecond flash-lamp (uF900) and a Xenon arc lamp (Xe900).

Acknowledgements

This work was supported by the National Key Research and Development Program of China (No. 2022YFA1405000), the National Natural Science Foundation of China (Nos. 62375141, T2488302 and 62405142), the Major Project of Natural Science Foundation of Jiangsu Province (No. 20243067), the Natural Science Foundation of Jiangsu Province (No. BK20240656), the China Postdoctoral Science Foundation (No. 2024M761391), and Special Funding for Chinese Postdoctoral Fellows (No. 2025T180229).

Conflicts of Interest

The authors declare no conflicts of interest.

Data Availability Statement

The data that supports the findings of this study are available in the supplementary material of this article.

References

1. J. Liu, Z. P. Song, J. Wei, et al., "Light-Dynamic Chirality Inversion of Circularly Polarized Organic Ultralong Room-Temperature Phosphorescence Enabled by Soft Helical Superstructure," *Advanced Optical Materials* 13 (2025): 2403468, https://doi.org/10.1002/adom.202403468.

2. J. Bao, R. Lan, C. Shen, et al., "Modulation of Chirality and Intensity of Circularly Polarized Luminescence Emitting From Cholesteric Liquid Crystals Triggered by Photoresponsive Molecular Motor," *Advanced Optical Materials* 10 (2021): 2101910, https://doi.org/10.1002/adom.202101910.

3. W. Kang, Y. Tang, X. Meng, et al., "A Photo- and Thermo-Driven Azoarene-Based Circularly Polarized Luminescence Molecular Switch in a Liquid Crystal Host," *Angewandte Chemie International Edition* 62 (2023): 202311486, https://doi.org/10.1002/anie.202311486.

4. J. Sun, R. Lan, Y. Gao, et al., "Stimuli-Directed Dynamic Reconfiguration in Self-Organized Helical Superstructures Enabled by Chemical Kinetics of Chiral Molecular Motors," *Advanced Science* 5 (2018): 1700613, https://doi.org/10.1002/advs.201700613.

5. H. K. Bisoyi and Q. Li, "Light-Directed Dynamic Chirality Inversion in Functional Self-Organized Helical Superstructures," *Angewandte Chemie International Edition* 55 (2016): 2994–3010, https://doi.org/10.1002/anie.201505520.

6. H. Li, H. Li, W. Wang, et al., "Stimuli-Responsive Circularly Polarized Organic Ultralong Room Temperature Phosphorescence," *Angewandte Chemie International Edition* 59 (2020): 4756–4762, https://doi.org/10.1002/anie.201915164.

7. Z. Huang, Z. He, B. Ding, H. Tian, and X. Ma, "Photoprogrammable Circularly Polarized Phosphorescence Switching of Chiral Helical Polyacetylene Thin Films," *Nature Communications* 13 (2022): 7841, https://doi.org/10.1038/s41467-022-35625-3.

8. L. Gu, W. Ye, X. Liang, et al., "Circularly Polarized Organic Room Temperature Phosphorescence from Amorphous Copolymers," *Journal of the American Chemical Society* 143 (2021): 18527–18535, https://doi.org/10.1021/jacs.1c08118.

9. B. Yue, X. Feng, C. Wang, et al., "In Situ Regulation of Microphase Separation-Recognized Circularly Polarized Luminescence via Photoexcitation-Induced Molecular Aggregation," *ACS Nano* 16 (2022): 16201–16210, https://doi.org/10.1021/acsnano.2c05056.

10. X. Wang, S. Ma, B. Zhao, and J. Deng, "Frontiers in Circularly Polarized Phosphorescent Materials," *Advanced Functional Materials* 33 (2023): 2214364, https://doi.org/10.1002/adfm.202214364.

11. K. Jiang, Q. Fan, D. Guo, C. Song, and J. Guo, "Circularly Polarized Room-Temperature Phosphorescence With an Ultrahigh Dissymmetry Factor From Carbonized Polymer Dots by Stacked Chiral Photonic Films," *ACS Applied Materials & Interfaces* 15 (2023): 26037–26046, https://doi.org/10.1021/acsami.3c04353.

12. Z. P. Song, J. Wei, J. Liu, et al., "Mechanically-Tunable and Full-Color Circularly Polarized Long-Lived Phosphorescence in Chiral Superstructure Elastomers," *Advanced Materials* 37 (2025): 2419640, https://doi.org/10.1002/adma.202419640.

13. F. Nie, K. Z. Wang, and D. Yan, "Supramolecular Glasses With Color-Tunable Circularly Polarized Afterglow Through Evaporation-Induced Self-Assembly of Chiral Metal–Organic Complexes," *Nature Communications* 14 (2023): 1654, https://doi.org/10.1038/s41467-023-37331-0.

14. J. Yan, F. Ota, B. A. San Jose, and K. Akagi, "Chiroptical Resolution and Thermal Switching of Chirality in Conjugated Polymer Luminescence via Selective Reflection Using a Double-Layered Cell of Chiral Nematic Liquid Crystal," *Advanced Functional Materials* 27 (2016): 1604529, https://doi.org/10.1002/adfm.201604529.

15. Y. He, S. Lin, J. Guo, and Q. Li, "Circularly Polarized Luminescent Self-Organized Helical Superstructures: From Materials and Stimulus-Responsiveness to Applications," *Aggregate* 2 (2021): 141, https://doi.org/10.1002/agt2.141.

16. Z. Zheng, H. Hu, Z. Zhang, et al., "Digital Photoprogramming of Liquid-Crystal Superstructures Featuring Intrinsic Chiral Photoswitches," *Nature Photonics* 16 (2022): 226–234, https://doi.org/10.1038/s41566-022-00957-5.

17. B. Liu, C. L. Yuan, H. L. Hu, et al., "Dynamically Actuated Soft Heliconical Architecture via Frequency of Electric Fields," *Nature Communications* 13 (2022): 2712, https://doi.org/10.1038/s41467-022-30486-2.

18. J. Bao, Z. Wang, C. Shen, et al., "Freestanding Helical Nanostructured Chiro-Photonic Crystal Film and Anticounterfeiting Label Enabled by a Cholesterol-Grafted Light-Driven Molecular Motor," *Small Methods* 6 (2022): 2200269, https://doi.org/10.1002/smtd.202200269.

19. X. Zhang, L. Li, Y. Chen, et al., "Mechanically Tunable Circularly Polarized Luminescence of Liquid Crystal-Templated Chiral Perovskite Quantum Dots," *Angewandte Chemie International Edition* 63 (2024): 202404202, https://doi.org/10.1002/anie.202404202.

20. J. Liu, Y. M. Qing, J. J. Wu, et al., "Responsive Cellulose Nanocrystal-Based Liquid Crystals: From Structural Color Manipulation to Applications," *Responsive Materials* 3 (2025): 70020, https://doi.org/10.1002/rpm2.70020.

21. C. Yuan, W. Huang, Z. Zheng, et al., "Stimulated Transformation of Soft Helix among Helicoidal, Heliconical, and Their Inverse Helices," *Science Advances* 5 (2019): aax9501, https://doi.org/10.1126/sciadv.aax9501.

22. Z. G. Zheng, Y. Li, H. K. Bisoyi, L. Wang, T. J. Bunning, and Q. Li, "Three-Dimensional Control of the Helical Axis of a Chiral Nematic Liquid Crystal by Light," *Nature* 531 (2016): 352–356, https://doi.org/10.1038/nature17141.

23. X. Wang, B. Zhao, and J. Deng, "Liquid Crystals Doped With Chiral Fluorescent Polymer: Multi-Color Circularly Polarized Fluorescence and Room-Temperature Phosphorescence With High Dissymmetry Factor and Anti-Counterfeiting Application," *Advanced Materials* 35 (2023): 2304405, https://doi.org/10.1002/adma.202304405.

24. S. Liu, X. Liu, Y. Wu, et al., "Circularly Polarized Perovskite Luminescence With Dissymmetry Factor up to 1.9 by Soft Helix Bilayer Device," *Matter* 5 (2022): 2319–2333, https://doi.org/10.1016/j.matt.2022.05.012.

25. J. Liu, X. Zhou, X. Tang, et al., "Circularly Polarized Organic Ultralong Room-Temperature Phosphorescence: Generation, Enhancement, and Application," *Advanced Functional Materials* 36 (2024): 2414086, https://doi.org/10.1002/adfm.202414086.

26. J. Liu, X. Y. Zhou, J. Wei, et al., "Multi-Color Circularly Polarized Room-Temperature Phosphorescence From Processable Chiral Photonic Films," *Advanced Functional Materials* 35 (2025): 2506911, https://doi.org/10.1002/adfm.202506911.

27. J. Liu, J. J. Wu, J. Wei, et al., "Dynamically Modulating the Dissymmetry Factor of Circularly Polarized Organic Ultralong Room-Temperature Phosphorescence from Soft Helical Superstructures," *Angewandte Chemie International Edition* 63 (2024): 202319536, https://doi.org/10.1002/anie.202319536.

28. R. Lan, J. Bao, Z. Li, et al., "A New Chirality Invertible Photoswitch: Light-Driven Axially Chiral Hydrazone Enabling Dynamic Handedness Inversion of Self-Organized Helical Superstructure," *Chinese Chemical Society Chemistry* 6 (2024): 2011–2020, https://doi.org/10.31635/ccschem.023.202303268.

29. P. Chen, L. L. Ma, W. Hu, et al., "Chirality Invertible Superstructure Mediated Active Planar Optics," *Nature Communications* 10 (2019): 2518, https://doi.org/10.1038/s41467-019-10538-w.

30. J. Wei, M. Zhu, T. Du, et al., "Full-Color Persistent Room Temperature Phosphorescent Elastomers With Robust Optical Properties," *Nature Communications* 14 (2023): 4839, https://doi.org/10.1038/s41467-023-40193-1.

31. H. Wang, H. K. Bisoyi, A. M. Urbas, T. J. Bunning, and Q. Li, "Reversible Circularly Polarized Reflection in a Self-Organized Helical Superstructure Enabled by a Visible-Light-Driven Axially Chiral Molecular Switch," *Journal of the American Chemical Society* 141 (2019): 8078–8082, https://doi.org/10.1021/jacs.9b03231.

32. X. Zhang, B. Koz, H. K. Bisoyi, et al., "Electro- and Photo-Driven Orthogonal Switching of a Helical Superstructure Enabled by an Axially Chiral Molecular Switch," *ACS Applied Materials & Interfaces* 12 (2020): 55215–55222, https://doi.org/10.1021/acsami.0c19527.

33. A. Ryabchun and A. Bobrovsky, "Cholesteric Liquid Crystal Materials for Tunable Diffractive Optics," *Advanced Optical Materials* 6 (2018): 1800335, https://doi.org/10.1002/adom.201800335.

34. Y. Li, M. Wang, T. J. White, T. J. Bunning, and Q. Li, "Azoarenes With Opposite Chiral Configurations: Light-Driven Reversible Handedness Inversion in Self-Organized Helical Superstructures," *Angewandte Chemie International Edition* 52 (2013): 8925–8929, https://doi.org/10.1002/anie.201303786.

35. H. Wang, Y. Tang, H. Krishna Bisoyi, and Q. Li, "Reversible Handedness Inversion and Circularly Polarized Light Reflection Tuning in Self-Organized Helical Superstructures Using Visible-Light-Driven Macrocyclic Chiral Switches," *Angewandte Chemie International Edition* 62 (2023): 202216600, https://doi.org/10.1002/anie.202216600.

36. H. Hayasaka, T. Miyashita, M. Nakayama, K. Kuwada, and K. Akagi, "Dynamic Photoswitching of Helical Inversion in Liquid Crystals Containing Photoresponsive Axially Chiral Dopants," *Journal of the American Chemical Society* 134 (2012): 3758–3765, https://doi.org/10.1021/ja2088053.

37. Y. Li, M. Wang, H. Wang, A. Urbas, and Q. Li, "Rationally Designed Axially Chiral Diarylethene Switches With High Helical Twisting Power," *Chemistry—A European Journal* 20 (2014): 16286–16292, https://doi.org/10.1002/chem.201403705.

38. M. Irie, T. Fukaminato, K. Matsuda, and S. Kobatake, "Photochromism of Diarylethene Molecules and Crystals: Memories, Switches, and Actuators," *Chemical Reviews* 114 (2014): 12174–12277, https://doi.org/10.1021/cr500249p.

39. A. Bosco, M. G. M. Jongejan, R. Eelkema, et al., "Photoinduced Reorganization of Motor-Doped Chiral Liquid Crystals: Bridging Molecular Isomerization and Texture Rotation," *Journal of the American Chemical Society* 130 (2008): 14615–14624, https://doi.org/10.1021/ja8039629.

40. M. J. Moran, M. Magrini, D. M. Walba, and I. Aprahamian, "Driving a Liquid Crystal Phase Transition Using a Photochromic Hydrazone," *Journal of the American Chemical Society* 140 (2018): 13623–13627, https://doi.org/10.1021/jacs.8b09622.

41. B. Balamut, R. P. Hughes, and I. Aprahamian, "Tuning the Properties of Hydrazone/Isosorbide-Based Switchable Chiral Dopants," *Journal of the American Chemical Society* 146 (2024): 24561–24569, https://doi.org/10.1021/jacs.4c07848.

42. I. Bala, J. T. Plank, B. Balamut, D. Henry, A. R. Lippert, and I. Aprahamian, "Multi-Stage and Multi-Colour Liquid Crystal Reflections Using a Chiral Triptycene Photoswitchable Dopant," *Nature Chemistry* 16 (2024): 2084–2090, https://doi.org/10.1038/s41557-024-01648-0.

43. S. Li, Y. Tang, Q. Fan, et al., "When Quantum Dots Meet Blue Phase Liquid Crystal Elastomers: Visualized Full-Color and Mechanically-Switchable Circularly Polarized Luminescence," *Light: Science & Applications* 13 (2024): 140, https://doi.org/10.1038/s41377-024-01479-1.

44. Y. Wu, M. Li, Z. G. Zheng, Z. Q. Yu, and W. H. Zhu, "Liquid Crystal Assembly for Ultra-dissymmetric Circularly Polarized Luminescence and Beyond," *Journal of the American Chemical Society* 145 (2023): 12951–12966, https://doi.org/10.1021/jacs.3c01122.

45. S. Lin, Y. Tang, W. Kang, H. K. Bisoyi, J. Guo, and Q. Li, "Photo-triggered Full-Color Circularly Polarized Luminescence Based on Photonic Capsules for Multilevel Information Encryption," *Nature Communications* 14 (2023): 3005, https://doi.org/10.1038/s41467-023-38801-1.

46. W. Huang, C. Fu, Z. Liang, K. Zhou, and Z. He, "Frontispiece: Strong Circularly-Polarized Room-Temperature Phosphorescence From a Feasibly Separable Scaffold of Bidibenzo[*b,d*]furan With Locked Axial Chirality," *Angewandte Chemie International Edition* 61 (2022): 202202977, https://doi.org/10.1002/anie.202202977.

47. Q. Fan, Z. Li, K. Jiang, J. Gao, S. Lin, and J. Guo, "Tunable Circular Polarization Room Temperature Phosphorescence With Ultrahigh Dissymmetric Factor by Cholesteric Liquid Crystal Elastomers," *Cell Reports Physical Science* 4 (2023): 101583, https://doi.org/10.1016/j.xcrp.2023.101583.

48. X. Zhang, Y. Xu, C. Valenzuela, et al., "Liquid Crystal-Templated Chiral Nanomaterials: From Chiral Plasmonics to Circularly Polarized Luminescence," *Light: Science & Applications* 11 (2022): 223, https://doi.org/10.1038/s41377-022-00913-6.

Supporting Information

Additional supporting information can be found online in the Supporting Information section.

Supporting File: adma73466-sup-0001-SuppMat.doc.